Journal of Applied Fluid Mechanics, Vol. 16, No. 10, pp. 1916-1926, 2023.
Available online at www.jafmonline.net, ISSN 1735-3572, EISSN 1735-3645.
https://doi.org/10.47176/jafm.16.10.1882

Dynamics of Microbubbles Oscillating in Rheopectic Fluids Subject to Acoustic Pressure Field

A. Abdollahi[1], A. Rafiei[1], M. Ahmadi[1], M. Pourjafar-Chelikdani[2†] and K. Sadeghy[1]

[1]*Department of Mechanical Engineering, University of Tehran, Tehran, Iran*
[2]*Caspian Faculty of Engineering, College of Engineering, University of Tehran, P.O. Box: 43841-119, Rezvanshahr, Iran*

†Corresponding Author Email: m_pourjafar@ut.ac.ir

ABSTRACT

In the present work, the dynamics of a single spherical gas bubble surrounded by a rheopectic fluid obeying the Quemada model is numerically investigated while the bubble undergoes oscillatory motion due to acoustic forcing. The generalized form of the Rayleigh–Plesset equation has been used for studying bubble dynamics in Quemada fluids. The integro-differential equation representing the dynamics of the bubble is solved numerically using the finite-element method (FEM) and also the Gauss–Laguerre quadrature (GLQ) method. The effect of rheopexy number (Rx) and viscosity ratio (ξ) are then investigated over a wide range of working parameters. Numerical results show that the rheopectic behavior of the fluid surrounding the bubble can dramatically affect the bubble dynamics. It is predicted that for highly anti-thixotropic fluids, harmonics are affected so much so that the bubble may exhibit chaotic behavior. For instance, at $Rx = 0.001$ and $\xi = 1/81$, a one-micron-sized bubble may attain a size almost 30 times of its initial size. The general conclusion is that, in sonography, microbubbles dispersed in rheopectic fluids may indeed be considered as a potent ultrasound contrast agent provided that the fluid is just moderately anti-thixotropic otherwise its chaotic response might damage the adjacent tissues.

Article History

Received March 21, 2023
Revised May 18, 2023
Accepted June 5, 2023
Available online July 29, 2023

Keywords:

Gas bubble
Rayleigh–Plesset equation
Acoustic pressure
Rheopectic fluid
Quemada model

1. INTRODUCTION

Bubble dynamics has historically been an active field of research due mainly to its application in cavitating flows (Mukundakrishnan et al., 2009; Andonova & Sekhar, 2016; Battistella et al., 2017; Dollet et al., 2019). It is also of widespread application in refrigeration and thermal systems where bubble dynamics normally involves heat and/or mass transfer (Dai et al., 2023). In recent years, interest in bubble dynamics has dramatically increased when it was realized that they can be used for opening the blood-brain-barrier (BBB) so that medication can reach the brain (McDannold et al., 2006; Liu et al., 2014). Further interest in bubble dynamics is related to its novel application as contrast agent in sonography (Nesser et al., 2002; Canchi et al., 2017). While cavitating flows usually involves Newtonian fluids, in many other cases of practical importance, the working fluid is realized to be non-Newtonian (Kelly, 2008; Saththasivam et al., 2016; Shpak et al., 2016; Sheeran et al., 2017; Chakibi et al., 2018; Dudek & Øye, 2018; Perera et al., 2018; Segers et al., 2018). For example, industrial fluids such as waxy crude oils and polymeric liquids are known to be non-Newtonian. This is also true for physiological fluids such as blood, saliva, mucus, and synovia that are known exhibit a variety of non-Newtonian behavior.

Due to its broad technological impact, bubble dynamics in non-Newtonian fluids has been the subject of many studies in the past. One can mention, for example, the work by Chahine et al. (2009) who investigated the response of gas bubbles in the whole blood modelled as a viscoelastic fluid. The elastic behavior of the blood was found to play a key role in bubble dynamics and its chaotic behavior when subjected to acoustic forcing; see, also, Cunha & Albernaz (2013). Zhang and Li (2014) numerically showed that during radial oscillations of gas bubbles, mass transfer is also affected by the elastic stresses generated in the liquid surrounding the bubble (Jim'enez-Fernandez & Crespo, 2005; Warnez & Johnsen, 2015). There are also several works addressing a fluid's yield stress on the bubble response (see, for example, Karapetsas, et al., 2019) where translational motion of the bubbles has been

NOMENCLATURE

r	radial coordinate	We	Weber number
t	time	Bo	Bond number
R	bubble radius	Rx	Rheopexy number
R_0	bubble initial radius	Γ	surface tension
$\dot{R}$	bubble radial velocity	$\dot{\gamma}$	shear rate
$\ddot{R}$	bubble acceleration	α	viscosity ratio
$P_{0,g}$	initial pressure of the gas trapped in the bubble	β	controlling parameter of Quemada model
$P_{0,\infty}$	initial far-field pressure	ω	frequency of far field acoustic pressure's oscillations
S	structural parameter of Quemada model	ε	amplitude of far field acoustic pressure's oscillations
S_0	initial structural parameter	ξ	viscosity ratio
a	microstructures rebuild controlling parameter	ρ	fluid density
b	microstructures breakdown controlling parameter	λ	structural time dependency controlling parameter
m	controlling parameter of Quemada model	μ_0	zero-shear viscosity (rebuild viscosity)
n	controlling parameter of Quemada model	μ_∞	infinite-shear viscosity (breakdown viscosity)
Cp	pressure coefficient	τ_{rr}	radial stress
Re	Reynolds number	$\tau_{\theta\theta}$	tangential stress

observed to be influenced by the liquid's yield stress. The effect of shear-thinning behavior of the fluid surrounding the bubbles has also been addressed in the past by Shima & Tsujino (1981) for unbounded domains. In a recent work, Arefmanesh et al. (2022), have investigated the effect of shear-thinning on a confined gas bubble and showed that the wall adjacent to the bubble can dramatically affect its dynamics. Surprisingly, work on bubble dynamics in time-dependent liquids is quite limited.

Time-dependent fluids are those fluids whose viscosity changes with time even at a given shear rate. Physiological fluids such as blood, and industrial fluids such as drilling muds, are known to exhibit significant time-dependent behavior. The main cause of time-dependent behavior is the fact that such fluids contain dispersed particles that form large-scale microstructures through inter-particle forces. These microstructures break down under shear that convert them into smaller structural units. This breakdown is simultaneously counter-balanced by the Brownian forces which try to rebuild the microstructures. This time-dependent breakdown and buildup of microstructures often result in a time-decaying viscosity known as thixotropy. And they have been the subject of several studies in recent years (Sadeghy & Vahabi, 2016; Moseley et al., 2019; Wang et al., 2020). One can particularly mention the works by Ahmadpour et al. (2011, 2014) on bubble dynamics in thixotropic fluids. They numerically showed that, under certain working conditions, a bubble's response is significantly affected by the time scale introduced through a fluid's thixotropic behavior.

Not all time-dependent fluids are thixotropic. There are fluids that exhibit anti-thixotropic behavior. Such fluids (which are often called rheopectic fluids) have a viscosity that increases with time even at a given shear rate—apparently because when microstructures are broken down, larger micelles and/or networks are formed. There are physiological and industrial fluids which exhibit rheopectic behavior. Synovial fluid in human joints, for example, exhibits this behavior. For such materials, as soon as the microstructures are broken down, they are interlinked with adjacent microstructures forming a new but *larger* microstructure. In practice, this phenomenon gives rise to an increase in the viscosity with time (Theodore et al., 2017). A review of studies carried out on bubble dynamics in the past indicated a lack of research on bubble behavior inside anti-thixotropic fluids. With this in mind, the present work aims at investigating the effect of a fluid's rheopectic behavior on the dynamics of a free gas bubble in an acoustic field, to the best of our knowledge, for the first time. To represent rheopectic fluids we rely on the Quemada rheological model. We are primarily interested in investigating the effect of anti-thixotropic behavior on the rise of harmonics in the bubble's response. This is because, in real world, harmonics are generated by bubbles not tissues surrounding them. In practice, this can help to detect the presence of bubbles in tiny blood vessels thereby significantly enhancing the quality of ultrasound images (Ahmadpour, et al., 2011). The fact that there are electronic devices in the market that can easily record second harmonics during bubble oscillation makes this technique highly attractive for next-generation sonography.

In the next section, the equations of motion together with the rheological model for the Quemada fluid are presented. This is followed by briefly describing the numerical solution used for solving the governing equations. Numerical results are presented next in which the effect of a fluid's time-dependent behavior is investigated on the bubble dynamics.

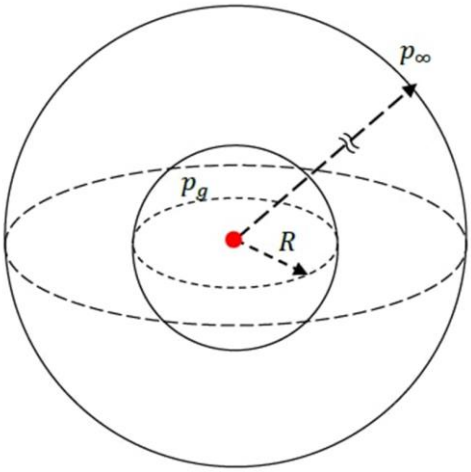

Fig. 1 Schematic showing a spherical gas bubble and the physical infinity

2. MATHEMATICAL FORMULATION

Figure 1 schematically shows the spherical free gas bubble at t = 0. This figure also shows the computational domain, which is spherical in shape with its radius placed at (physical) infinity. We assume that the bubble is occupied by a perfect non-condensable gas. We also assume that the bubble always remains spherical during its motion, which tacitly means that the effect of the gravitational force on the bubble is negligible. The liquid surrounding the bubble is assumed to be incompressible and time-dependent.

Since the bubble remains always spherical, the velocity induced in the liquid during bubble motion, $v_r(r,t)$, is purely radial. Based on the continuity equation, the radial velocity induced in the liquid at an arbitrary radius (r) can then be obtained as: $v_r(r,t) = R^2\dot{R}/r^2$ where R is the bubble radius with $\dot{R}$ being its surface velocity. The r-momentum equation (in spherical coordinate system then becomes (Plesset, 1949):

$$\rho\left(\frac{R^2\ddot{R}+2R\dot{R}}{r^2}-\frac{2R^4\dot{R}^2}{r^5}\right) = -\frac{\partial p}{\partial r}+\frac{\partial \tau_{rr}}{\partial r}+ 2\left(\frac{\tau_{rr}-\tau_{\theta\theta}}{r}\right). \quad (1)$$

where τ_{rr} and $\tau_{\theta\theta}$ are, respectively, the radial and tangential stresses. The equation governing the bubble dynamics can then be obtained by integrating this equation from the surface of the bubble up to the infinity having assumed that the non-condensable gas inside the bubble undergoes a polytropic process (Plesset, 1949); that is:

$$\rho\left(R\ddot{R}+\frac{3}{2}\dot{R}^2\right) = p_{g,0}\left(\frac{R_0}{R}\right)^{3\kappa} - p_\infty(t) - \frac{2\Gamma}{R}+2\int_R^\infty\left(\frac{\tau_{rr}-\tau_{\theta\theta}}{r}\right)dr. \quad (2)$$

where $\ddot{R}$ is the acceleration of the bubble. ρ is the fluid density, Γ is the surface tension, and κ is the polytropic constant. Subscript g and zero refer to the gas and initial conditions, respectively. Also, p_∞ refers to the pressure at infinity. Equation (2) is the general form of the Rayleigh–Plesset (RP) equation. It models the motion of a spherical free gas bubble in an incompressible liquid, whether Newtonian or non-Newtonian (Allen & Roy, 2000a). It assumes that at infinity the fluid is at rest and all stress terms are equal to zero. To un-balance the bubble, the pressure at infinity has to be varied (Rayleigh, 1917). In the present work, the bubble is subjected to an acoustic pressure field; that is:

$$p_\infty(t) = p_{\infty,0}\left[1+\varepsilon\sin(\omega t)\right] \quad (3)$$

where ε is the perturbation to the initial pressure at infinity, $p_{\infty,0}$. For non-Newtonian fluids, one has to decide on the rheological model so that the stress terms in Eq. (2) can be related to the bubble radius. In the present work, we assume that the fluid obeys the Quemada model. It is a robust rheological model and is widely used to represent shear-dependent fluids that simultaneously exhibit a time-dependent viscosity. Quemada model incorporates a structural parameter (S) which varies between 0 and 1 depending on the state of the internal microstructures being fully destructed (S = 0) or fully rebuilt (S = 1), respectively. The apparent viscosity (η) of the fluid depends on S and also the shear rate, as shown below (Quemada, 1984):

$$\eta(S,\dot{\gamma}) = \mu_\infty(1+\alpha S)^\beta. \quad (4)$$

where μ_∞ is the infinite-shear viscosity (corresponding to $S = 0$) with $\mu_0 = \mu_\infty(1+\alpha)^\beta$ being the zero-shear viscosity (corresponding to S = 1). The structural parameter itself satisfies the following kinetic equation:

$$\frac{DS}{Dt} = a(1-S)\dot{\gamma}^m - bS\dot{\gamma}^n. \quad (5)$$

where D/Dt is the material derivative. In Quemada model, "a" represents structure rebuild (by Brownian motions) while "b" controls the rate at which microstructures are broken down by the deformation field where $\dot{\gamma}$ is the *effective* shear rate defined as:

$$\dot{\gamma} = \sqrt{|II_{\dot{\gamma}}|} = 2\sqrt{3}\left|\frac{R^2\dot{R}}{r^3}\right|. \quad (6)$$

where $II_{\dot{\gamma}}$ is the second invariant of the deformation-rate tensor. A close look at Eq. (4) reveals that, for the model to represent a time-dependent fluid it is required that we should have: $\alpha \neq 0$ and $\beta \neq 0$. In fact, the Quemada model reduces simply to the Newtonian fluid model (with viscosity μ_∞) by setting $\alpha = 0$. Using the stress terms for the Quemada model (Abdollahi, 2019), the generalized Rayleigh-Plesset equation is obtained as:

$$\rho\left(R\ddot{R}+\frac{3}{2}\dot{R}^2\right)=\left(p_{0,\infty}+\frac{2\Gamma}{R_0}\right)\left(\frac{R_0}{R}\right)^{3\kappa}- \quad (7)$$
$$p_{0,\infty}\left[1+\varepsilon\sin(\omega t)\right]-\frac{2\Gamma}{R}-$$
$$12R^2\dot{R}\mu_\infty\int_R^\infty\frac{(1+\alpha S)^\beta}{r^4}dr.$$

It is important to note that, Quemada model can represent both thixotropic and anti-thixotropic fluids. For the latter fluids, however, the infinite-shear viscosity is larger than the zero-shear viscosity $\mu_\infty > \mu_0$. In other words, when equilibrium is reached, a rheopectic fluid always attains a larger viscosity than its initial viscosity. It can be shown that, for the model to represent anti-thixotropic fluids we should have $\alpha\beta < 0$. To show this we can integrate Eq. (5) at a constant shear rate to obtain the time-evolution of structural parameter (for $S_0 = 1$):

$$S(t,\dot{\gamma})=\frac{1-exp\left[-a\left(\dot{\gamma}^m+(b/a)\dot{\gamma}^n\right)t\right]}{1+\dot{\gamma}^{(n-m)}/a}+ \quad (8)$$
$$\exp\left[-a\left(\dot{\gamma}^m+(b/a)\dot{\gamma}^n\right)t\right]\ .$$

Having obtained S from Eq. 8, Eq. 4 can be used to obtain the apparent viscosity as a function of time. As can be seen in Fig. 2, at short times, the exponential term in Eq. 8 dominates but eventually viscosity reaches an asymptotic value. More importantly, based on this figure, the apparent viscosity increases with time as long as $\alpha\beta < 0$. For most physiological fluids (e.g., synovia) α is a positive number. As such, with no loss of generality, in our simulation β is assigned negative values (e.g., $\beta = -2$) so that Quemada model can represent rheopectic fluids

2.1 Dimensionless Numbers

Equation (7) can be made dimensionless using R_0 as the length scale, $1/\omega$ as the time scale, and ωR_0 as the velocity scale. The results is:

$$\left(R\ddot{R}+\frac{3}{2}\dot{R}^2\right)=C_P\left[\begin{matrix}(1+We)\left(\frac{1}{R}\right)^{3\kappa}-\\(1+\varepsilon\sin(t))-\frac{We}{R}\end{matrix}\right]- \quad (9)$$
$$\frac{12R^2\dot{R}}{Re}\int_R^\infty\frac{(1+\alpha S)^\beta}{r^4}dr.$$

where we have:

$$Cp=\frac{p_{\infty,0}}{\rho R_0^2\omega^2}\ ;\ We=\frac{2\Gamma}{p_{\infty,0}R_0}\ ;\ Re=\frac{\rho\omega R_0^2}{\mu_\infty}. \quad (10)$$

where C_p is the pressure coefficient, which can be interpreted as the pressure force divided by the temporal inertial force; it is varied through varying ε. On the other hand, *We* is the nominal Weber number and is interpreted as the surface tension force divided by the pressure force; it is varied through varying the surface tension, Γ. Finally, *Re* is the Reynolds number which, here, compares temporal inertial force with the viscous force, and so it can be interpreted as the Womersley number. In this work, it is varied through varying frequency, ω. We can also define a Bond number (*Bo*), as shown below:

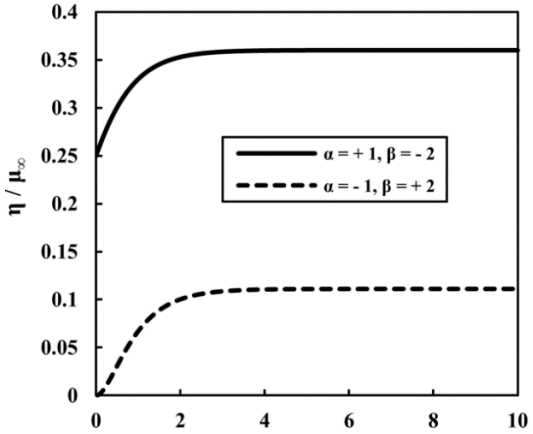

Fig. 2 Effect of αβ on the normalized viscosity ($m = 0$, $n = 0.5$, $S_0 = 1$, $a = 1$, $b = 0.5$, $\dot{\gamma} = 1$).

$$Bo=\frac{\Delta\rho g R_0^2}{\Gamma}, \quad (11)$$

which signifies the competition between gravitational force with the surface tension force. For the micron-sized bubbles used in this study, *Bo* is vanishingly small ensuring that the effect of gravity is indeed negligible confirming that the bubble always remains spherical. Using the scales mentioned above, the Quemada model can also be made dimensionless as:

$$\lambda\left(\frac{\partial S}{\partial t}+v_r\frac{\partial S}{\partial r}\right)=-\mathrm{Rx}\ \dot{\gamma}^n S+\dot{\gamma}^m(1-S). \quad (12)$$

where,

$$\lambda=\frac{\omega^{1-m}}{a}\ ;\ Rx=\left(\frac{b}{a}\right)\omega^{n-m}. \quad (13)$$

Evidently, λ and *Rx* both represent time-dependency of the fluid because they both involve "*a*". But, because *Rx* simultaneously involves "*b*", it is a better measure of time-dependency. As such, with no loss of generality, we arbitrarily set $\lambda = 1$ while *Rx* (called the *rheopexy* number) is varied over a broad range. Results obtained at very low rheopexy numbers (*Rx*) are representative of strong thixotropic/rheopectic effects whereas results obtained at very high *Rx* numbers highlight the role played by the shear-dependent viscosity of the fluid. We can also define a viscosity ratio, as shown below:

$$\xi=\mu_0/\mu_\infty=(1+\alpha)^\beta. \quad (14)$$

Since for anti-thixotropic fluids we have $\mu_\infty > \mu_0$, one can conclude that for such fluids $\xi < 1$.

3. NUMERICAL METHOD

Equations (9) and (12) have no analytical solution in close sight. As such, they should be solved numerically. A good option is the Gauss-Laguerre quadrature (GLQ)

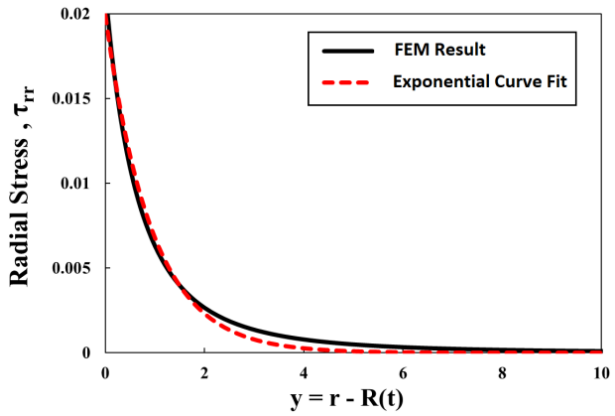

Fig. 3 Variation of τ_{rr} in the radial direction for Quemada fluids at dimensionless time t* = 6. This figure shows that the exponential fit is reasonably good (m = 0, n = 0.5, β = -2, Re = 100, C_p = 4, ϵ = 1, We = 0.03, ξ = 4/49, Rx = 0.001)

method, which was used extensively in the past for simulating the dynamics of spherical gas bubbles oscillating in thixotropic fluids (Ahmadpour et al., 2011, 2014). The GLQ method, however, is based on the premise that the radial normal stress generated in the liquid decays exponentially with distance from the bubble so that the integral term in Rayleigh-Plesset equation can be approximated by Laguerre polynomials. But, this premise is not necessarily true for all non-Newtonian fluids. To see if it is indeed true for Quemada model, use was made of the finite element software package COMSOL Multiphysics (V5.5). Based on Fig. 3, the exponential fit is realized to be indeed a good approximation to the radial stress. Note that y in Fig. 3 represents the distance from a wrbitrary node in the horizonthal direction to the surface of the bubble; see Appendix A for more details.

The notion that exponential decay of radial stress is indeed a good approximation for Quemada model is seen in Fig. 4 that shows a comparison between our FEM and GLQ codes; see Appendix B. The difference between the two numerical methods is seen to be quite negligible.

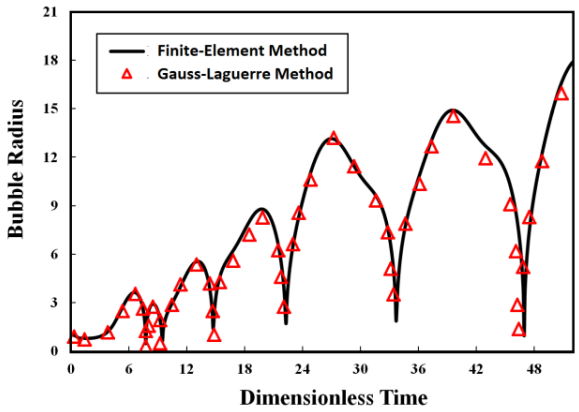

Fig. 4 A typical comparison between our FEM and GLQ codes for Moore thixotropic fluids. (m = 0, n = 1, β = 1, C_p = 4, ϵ = 2, Re = 5.5, We = 0.2, ξ = 1/121, Rx = 10)

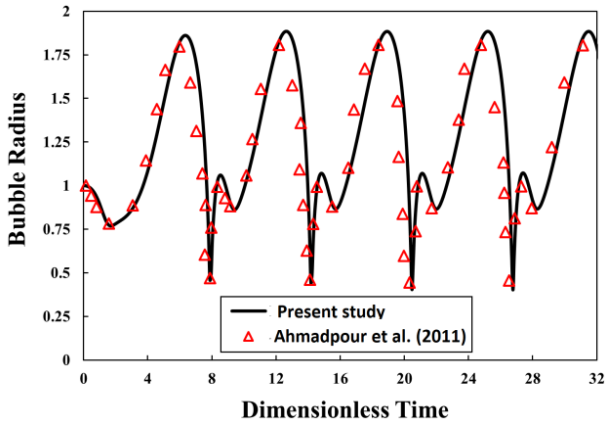

Fig. 5 Verification with published numerical data for the Moore thixotropic model (m = 0, n = 1, β = 1, C_p = 4, ϵ = 2, Re = 5.5, We = 0.2, ξ = 1/121, Rx = 10)

In fact, the FEM code/script developed in the present work in COMSOL environment could easily recover all GLQ numerical results reported by Ahmadpour et al. (2011) for the Moore thixotropic model, which is a special form of the Quemada model (m = 0, n = 1, β = 1). Figure 5 shows a typical comparison between the two sets of numerical results. The comparison is very good, although it can be argued that the FEM results are more accurate because unlike the GLQ method FEM method does not have to enforce S = 1 boundary condition upfront; see Appendix A for more details.

4. RESULTS AND DISCUSSION

Having verified the code, it was used to investigate the response of the bubble in Quemada model for model parameters representing rheopectic fluids. In terms of the dimensionless numbers, the inputs are Re, We, Cp, Rx, and ξ. And the output is the dimensionless (R^*) radius as a function of dimensionless time (t^*). The main objective is to investigate the effect of the rheopexy number (Rx) on the bubble dynamics because it has not been investigated in the past, whether theoretically or experimentally. Still, the problem involves too many parameters with some of them addressed in previous works. As such, we arbitrarily set m = 0, n = 0.5, β = –2, We = 0.03, λ = 1 and ε = 1. Unless otherwise stated, Re is fixed at 1. The main objective of the work is to investigate the effect of Rx although the effect of viscosity ratio, ξ is also investigated.

4.1 Effect of Rheopexy Number, *Rx*

As earlier mentioned, the rheopexy number (Rx) represents the rheopectic behavior of the Quemada model because it involves the b/a ratio; see Eq. (13). Figure 6 shows the strong effect of Rx number on the bubble response. The plots also include Newtonian results for comparison purposes. The figure shows that deviation from Newtonian behavior becomes progressively more severe the smaller the Rx number, i.e., when the fluid becomes more rheopectic. Based on the results shown in Fig. 6, the competition between the time scale of acoustic forcing (represented by ω^{-1}), the time scale of

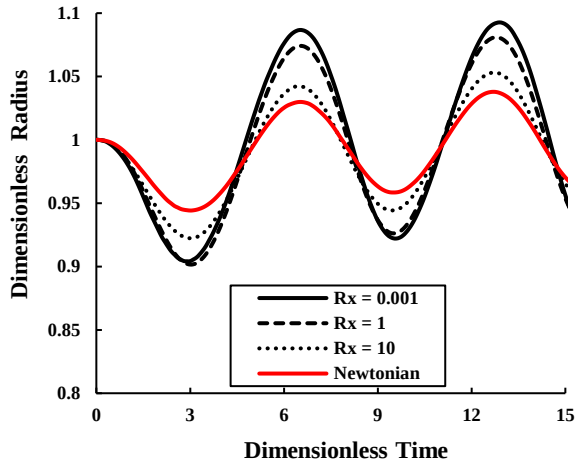

(a)

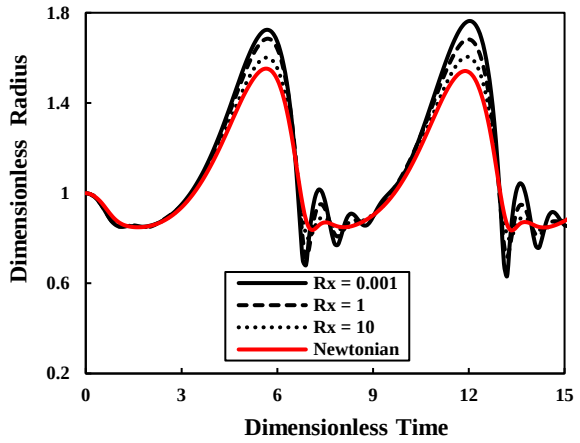

(b)

Fig. 6 Effect of rheopexy number (*Rx*) on the bubble's response to acoustic pressure. (*Re* = 1, ξ = 4/9: (a) C_p = 0.16; (b) C_p = 4)

the deformation time of the fluid (represented by the *b/a* ratio) can strongly affect the bubble response with its severity controlled by the *Cp*.

Another look at Fig. 6b reveals that for *Cp* = 4 the harmonics are strongly affected by the *Rx* number. To show this in better perspective, Fig. 7 shows a zoomed view of Fig. 6b. As is seen in this figure, the time at which the bubble radius successively peaks is closely controlled by *Rx*. More importantly, new harmonics are generated for the Quemada fluids as compared with the Newtonian fluids.

The results shown in Fig. 6 clearly demonstrate that at *Re* = 1 the bubble response is periodic. Figure 8 shows that this is not necessarily true at *Re* = 100. In fact, as compared with the Newtonian fluids, the chaotic behavior becomes stronger the smaller the *Rx* number. In other words, fluids that are extremely rheopectic are more prone to chaotic behavior—a phenomenon which is a clear manifestation of shape instability.

The prediction that the Reynolds number has a strong effect on the bubble response is nothing new and is well-established in the literature (Sokolov et al., 2000). An increase in the Re means that the nonlinear inertial terms are becoming larger, and so shape instability may easily occur, which manifests

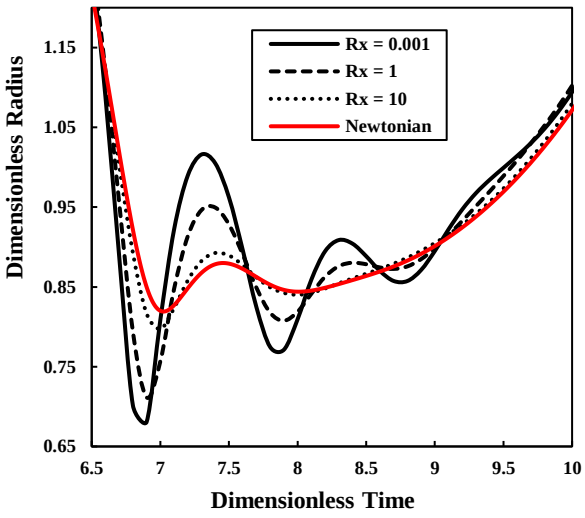

Fig. 7 Effect of rheopexy number (*Rx*) on the harmonics (*Re* = 1, ξ = 4/9, C_p = 4)

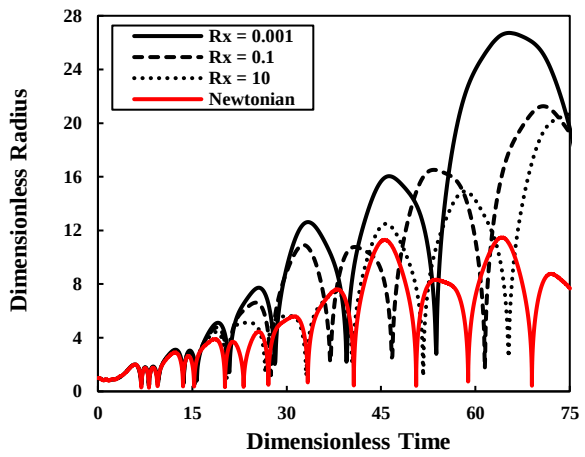

Fig. 8 Effect of rheopexy number (*Rx*) on the bubble's response to acoustic pressure (*Re* = 100, ξ = 4/9, *Cp* = 4

itself as the chaotic behavior (Sokolov et al., 2000). This is actually the main reason for the chaotic behavior for Newtonian fluids, which have a linear constitutive behavior. The situation becomes much more severe for nonlinear fluids such as those obeying the Quemada model—which become more nonlinear the smaller the *Rx* number. For such fluids, the chaotic behavior exhibits itself by a dramatic increase in the bubble radius. Specifically, for *Rx* = 0.001 and ξ = 1/81, a one-micron-sized bubble attains a size almost 30 times its initial radius.

4.2 Effect of Viscosity Ratio, ξ

Figure 9 shows the effect of viscosity ratio (ξ) in the rheopectic fluid (ξ < 1) for two different pressure coefficients.

The results presented in Fig. 9 depict the strong effect of the pressure coefficient on bubble dynamics. The effect was anticipated because an increase in *Cp* means an increase in the amplitude of the acoustic forcing which

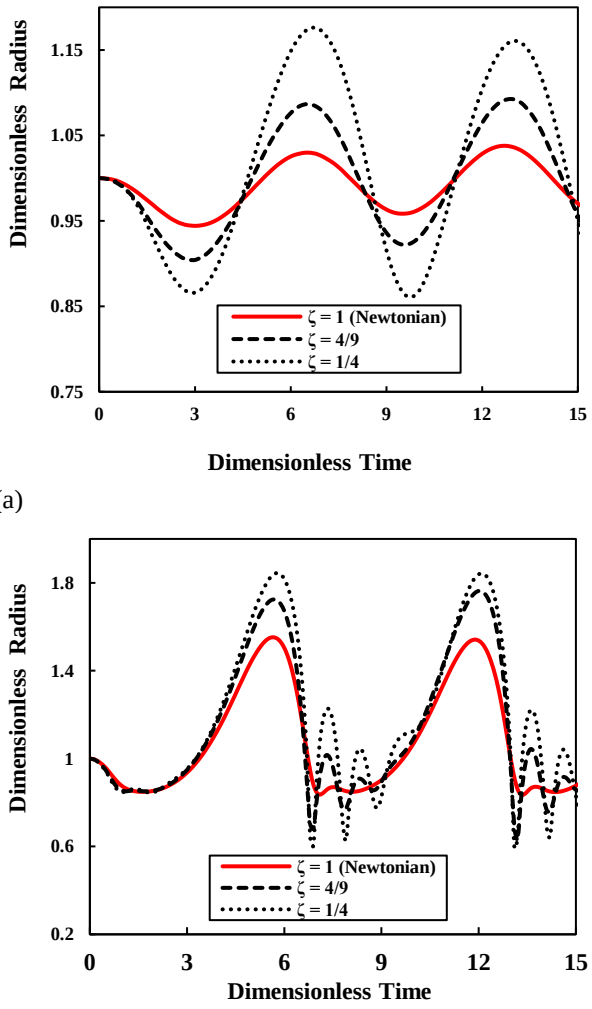

Fig. 9 Effect of viscosity ratio (ξ) on the bubble's response to acoustic pressure (*Rx* = 0.001, *Re* = 1: (a) *Cp* = 0.16; (b) *Cp* = 4)

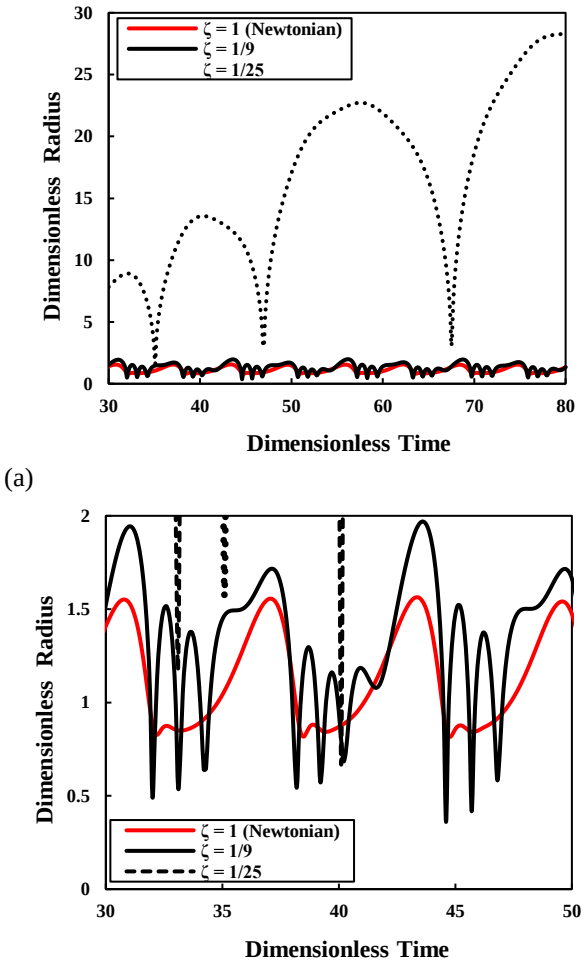

Fig. 10 (a) Effect of viscosity ratio on the bubble's response to acoustic pressure; (b) zoomed view (*Re* = 1, *Rx* = 0.001, *Cp* = 4)

makes the response increasingly more nonlinear. The response of the bubble is seen to be periodic although for *Cp* = 4 harmonics are predicted to arise in the response of the bubble. The harmonics in Fig. 9 are seen to be controlled by ξ. The strong effect of ξ on the bubble response is not surprising because by reducing this ratio the difference between μ_0 and μ_∞ is progressively increased. As a result, the fluid needs more time to reach μ_∞ and, in practice, it translates itself into a stronger anti-thixotropic behavior, as can be seen in Fig. 9. If this explanation is true, it is speculated that for sufficiently small viscosity ratios, the response should become chaotic. Figure 10 shows that this is indeed the case.

Figure 10a shows that the chaotic behavior becomes more sever the smaller the viscosity ratio. For example, for the extreme case of ξ = 1/81, a one-micron-sized bubble acquires a size almost 30 times its initial radius provided that the *Rx* number is sufficiently small (say, 0.001). Interestingly, for the same set of parameters, a Newtonian fluid does not exhibit any chaotic behavior; see Fig. 10b.

5. CONCLUDING REMARKS

In the present work, the behavior of a tiny gas bubble surrounded by a time-dependent fluid obeying the Quemada model has been numerically investigated. For numerically solving the equations of motion, use was made of the Gauss-Laguerre method. Based on the obtained numerical results, the following conclusions are made:

- Anti-thixotropy of the Quemada model represented by the rheopexy number affect the bubble response with its severity depending on the amplitude and frequency of the acoustic wave.
- For sufficiently large amplitudes and frequencies the response of the bubble is predicted to be periodic regardless of the rheopexy number.
- At sufficiently high Reynolds numbers, the response of the bubble becomes chaotic with its severity controlled by the viscosity ratio.
- Microbubbles can be used as effective ultrasound contrast agents for rheopectic physiological fluids such as synovia provided that the level of their anti-thixotropy is

not too severe otherwise chaotic response might emerge that might damage the tissues adjacent to the bubble.

Work is currently ongoing in our research group to determine the critical values for the rheopexy number through a proper linear temporal instability analysis.

ACKNOWLEDGEMENT

The authors would like to thank the respectful reviewers for their constructive comments. Special thanks are also due to INSF (Iran National Science Foundation) for supporting this work under contract # 93034827.

CONFLICT OF INTEREST

The authors have no conflicts to disclose.

AUTHORS CONTRIBUTION

A. Abdollahi: carried out the Guass-Lagerre simulations, prepared the figures; **A. Rafiei**: carried out the Guass-Lagerre simulations, prepared the figures; M. Ahmadi: carried out the Guass-Lagerre simulations, prepared the figures; **M. Pourjafar-Chelikdani**: Reviewed the first and second versions of the manuscript; co-supervised the work; carried out the COMSOL simulations, contributed to answering the comments. **K. Sadeghy**: wrote the first version of the manuscript; supervised the work; interpreted the results and contributed to answering the comments.

REFERENCES

Abdollahi, A., (2019). *Effect of rheopexy on the naturatural frequency of spherical bubbles subjected to acoustic pressure field*. [Masters thesis, Univeristy of Tehran].

Ahmadpour, A., Amini-Kafiabad, H., & Sadeghy, K. (2014). Dynamic of gas bubbles surrounded by a dullaert-mewis thixotropic fluid. *Nihon Reoroji Gakkaishi*, 41(5), 309-318. http://dx.doi.org/10.1678/rheology.41.309

Ahmadpour, A., Amini-Kafiabad, H., Samadi, J., & Sadeghy, K. (2011). The rise of second harmonics in forced oscillation of gas bubbles in thixotropic fluids. *Nihon Reoroji Gakkaishi*, 39(3), 113-117. https://doi.org/10.1678/rheology.39.113

Allen, J. S., & Roy, R. A. (2000). Dynamics of gas bubbles in viscoelastic fluids. I. Linear viscoelasticity. *The Journal of the Acoustical Society of America*, 107(6), 3167-3178. https://doi.org/10.1121/1.429344

Andonova, V., & Sekhar, G. C. (2016). Rise time Calculations of a single air bubble under the influence of gravity in a pool of water. *Journal of Applied Science and Engineering Methodologies*, 2(3), 426-434. http://jasem.in/2016/23426434.html#

Arefmanesh, A., Arani, M. M., & Arani, A. A. (2022). Dynamics of a bubble in a power-law fluid confined within an elastic Solid, *European Journal of Mechanics / B Fluids*, 94, 29–36. https://doi.org/10.1016/j.euromechflu.2022.02.002

Battistella, A., Van-Schijndel, S., Baltussen, M. W., Roghair, I., & Van-Sint-Annaland, M. (2017). *Front-tracking simulations of bubbles in non-newtonian fluids.* 12th International Conference on Computational Fluid Dynamics in the Oil & Gas, Metallurgical and Process Industries (CFD 2017), (pp. 469-478). SINTEF Academic Press. https://research.tue.nl/en/publications/front-tracking-simulations-of-bubbles-in-non-newtonian-fluids

Canchi, S., Kelly, K., Hong, Y., King, M. A., Subhash, G., & Sarntinoranont, M. (2017). Controlled single bubble cavitation collapse results in jet-induced injury in brain tissue. *Journal of the Mechanical Behavior of Biomedical Materials*, *74*, 261-273. http://dx.doi.org/10.1016/j.jmbbm.2017.06.018

Chahine, G. L., Tanguay, M., & Loraine, G. (2009). Acoustic measurements bubbles in biological tiessure. *Journal of Hydrodynamics*, 21(1), 47-64. https://doi.org/10.1016/S1001-6058(08)60118-3

Chakibi, H., Hénaut, I., Salonen, A., Langevin, D., & Argillier, J. F. (2018). Role of bubble–drop interactions and salt addition in flotation performance. *Energy & Fuels*, *32*(3), 4049-4056. https://doi.org/10.1021/acs.energyfuels.7b04053

Cunha, F. R. & Albernaz, D. L. (2013). Oscillatory motion of a spherical bubble in a non-Newtonian fluid. *Journal of Non-Newtonian Fluid Mechanics*, 191, 35-44. https://doi.org/10.1016/j.jnnfm.2012.10.010

Dai, B., Liu, C., Liu, S., Wang, D., Wang, Q., Zou, T., & Zhou, X. (2023). Life cycle techno-enviro-economic assessment of dual-temperature evaporation transcritical CO2 high-temperature heat pump systems for industrial waste heat recovery. *Applied Thermal Engineering*, 219, Part B, 119570. https://doi.org/10.1016/j.applthermaleng.2022.119570

Dollet, B., Marmottant, P., & Garbin, V. (2019). Bubble dynamics in soft and biological matter. *Annual Review of Fluid Mechanics*, 51, *331-355*. https://doi.org/10.1146/annurev-fluid-010518-040352

Dudek, M., & Øye, G. (2018). Microfluidic study on the attachment of crude oil droplets to gas bubbles. *Energy & Fuels*, 32(10), 10513-10521. http://hdl.handle.net/11250/2582618

Jaluria, Y. (1988). *Computer methods for engineering*, Allyn and Baycon Inc., Boston. https://www.amazon.com/Computer-Methods-Engineering-Allyn-Bacon/dp/0205106366

Jim'enez-Fernandez, J., & Crespo, A. (2005). Bubble oscillation and inertial cavitation in viscoelastic fluids. *Ultrasonics*, 43(8), 643-651. https://doi.org/10.1016/j.ultras.2005.03.010

Kafiabad, H. A., & Sadeghy, K. (2010). Chaotic behavior of a single spherical gas bubble surrounded by a

Giesekus liquid: A numerical study. *Journal of Non-Newtonian Fluid Mechanics*, 165(13-14), 800-811. http://dx.doi.org/10.1016/j.jnnfm.2010.04.010

Karapetsas, G., Photeinos, D., Dimakopoulos, Y., & Tsamopoulos, J. (2019). Dynamics and motion of a gas bubble in a viscoplastic medium under acoustic. *Journal of Fluid Mechanics*, 865, 381-413. https://doi.org/10.1017/jfm.2019.49

Kelly, W. J. (2008). Using computational fluid dynamics to characterize and improve bioreactor performance. *Biotechnology and applied biochemistry*, 49(4), 225-238. https://doi.org/10.1042/ba20070177

Liu, H. L., Fan, C. H., Ting, C. Y., & Yeh, C. K. (2014). Combining microbubbles and ultrasound for drug delivery to brain tumors: current progress and overview. *Theranostics*, 4(4), 432. https://doi.org/10.7150%2Fthno.8074

McDannold, N., Vykhodtseva, N., & Hynynen, K. (2006). Targeted disruption of the blood–brain barrier with focused ultrasound: association with cavitation activity. *Physics in Medicine & Biology*, 51(4), 793. https://doi.org/10.1088/0031-9155/51/4/003

Moseley, K., Fairweather, M. & Harbottle, D. (2019). Settling dynamics of two identical vertically aligned spheres in a thixotropic fluid. *Journal of Non-Newtonian Fluid Mechanics*, 271, 104146. https://doi.org/10.1016/j.jnnfm.2019.104146

Mukundakrishnan, K., Ayyaswamy, P. S. & Eckmann, D. M. (2009). Bubble motion in a blood vessel: shear stress induced endothelial cell injury. https://doi.org/10.1115/1.3153310

Nesser, H. J., Karia, D. H., Tkalec, W., & Pandian, N. G. (2002). Therapeutic ultrasound in cardiology. *Herz*, 27(3), 269-278. https://doi.org/10.1007/s00059-002-2362-y

Perera, R., Nittayacharn, P., Cooley, M., Jung, O., & Exner, A. A. (2018). Ultrasound contrast agents and delivery systems in cancer detection and therapy. *Advances in Cancer Research*, 139, 57-84. https://doi.org/10.1016/bs.acr.2018.04.002

Plesset, M. S. (1949). The dynamics of cavitation bubbles. *Journal of Applied Mechanics*. 16 (3), 228–231.https://doi.org/10.1115/1.4009975

Quemada, D. (1984). Towards a unified model of elasto-thixotropy of biofluids. *Biorheology*, 21(4), 423–436. https://doi.org/10.3233/bir-1984-21403

Rayleigh, L. (1917). On the pressure developed in a liquid during the collapse of a spherical cavity. *Phil. Mag*. 34 (200), 94–98. https://doi.org/10.1080/14786440808635681

Sadeghy, K., & Vahabi, M. (2016). The effect of thixotropy on a rising gas bubble: A numerical study. *Korea-Australia Rheology Journal*, 28(3), 207-216. http://dx.doi.org/10.1007/s13367-016-0021-8

Saththasivam, J., Loganathan, K., & Sarp, S. (2016). An overview of oil–water separation using gas flotation systems. *Chemosphere*, 144, 671-680. https://doi.org/10.1016/j.chemosphere.2015.08.087

Segers, T., Kruizinga, P., Kok, M. P., Lajoinie, G., De Jong, N., & Versluis, M. (2018). Monodisperse versus polydisperse ultrasound contrast agents: Non-linear response, sensitivity, and deep tissue imaging potential. *Ultrasound in Medicine & Biology*, 44(7), 1482-1492.https://doi.org/10.1016/j.ultrasmedbio.2018.03.019

Sheeran, P. S., Yoo, K., Williams, R., Yin, M., Foster, F. S., & Burns, P. N. (2017). More than bubbles: creating phase-shift droplets from commercially available ultrasound contrast agents. *Ultrasound in Medicine & Biology*, 43(2), 531-540. https://doi.org/10.1016/j.ultrasmedbio.2016.09.003

Shima, A., & Tsujino, T. (1981). The effect of polymer concentration on the bubble behavior and impulse pressure. *Chemical Engineering Science*, 36 (5), 931–935. https://doi.org/10.1016/0009-2509(81)85047-6

Shpak, O., Verweij, M., Jong, N. D., & Versluis, M. (2016). Droplets, bubbles and ultrasound interactions. *Therapeutic Ultrasound*, 880, 157-174.https://doi.org/10.1007/978-3-319-22536-4_9

Sokolov, I. V., Didenkulov, I. N., Selivanovsky, D. A., & Semenov, V. E. (2000*). Bubble Shape Instability in a Strong Acoustic Field*. AIP Conference Proceedings, 524, 371. https://doi.org/10.1063/1.1309244

Theodore, L., Dupont, R. R., & Ganesan, K. (2017). Unit operations in environmental engineering. *John Wiley & Sons.* https://www.wiley.com/en-us/Unit+Operations+in+Environmental+Engineering-p-9781119283706

Wang, Z., Ma, J., Gao, H., Stuedlein, A. W., He, J., & Wang, B. (2020). Unified thixotropic fluid model for soil liquefaction. *Géotechnique*, 70(10), 849-862. http://dx.doi.org/10.1680/jgeot.17.p.300

Warnez, M. T., & Johnsen, E. (2015). Numerical modeling of bubble dynamics in viscoelastic media with relaxation. *Physics of Fluids*, 27(6), 063103. https://doi.org/10.1063/1.4922598

Zhang, Y., & Li, S. (2014). Mass transfer during radial oscillations of gas bubbles in viscoelastic mediums under acoustic excitation. *International Journal of Heat and Mass Transfer*, 69, 106-116. http://dx.doi.org/10.1016/j.ijheatmasstransfer.2013.10.019

APPENDIX A: FINITE ELEMENT METHOD

COMSOL Multiphysics is known to be a versatile finite element software for solving complex fluid mechanics problems. The software is equipped with a robust, highly-efficient solver for partial-differential equations that can be used also for solving ordinary differential equations (ODE) through certain adjustments. All we have to do is to define the Rayleigh-Plesset equation (Eq. 9) together with the kinetic equation (Eq.

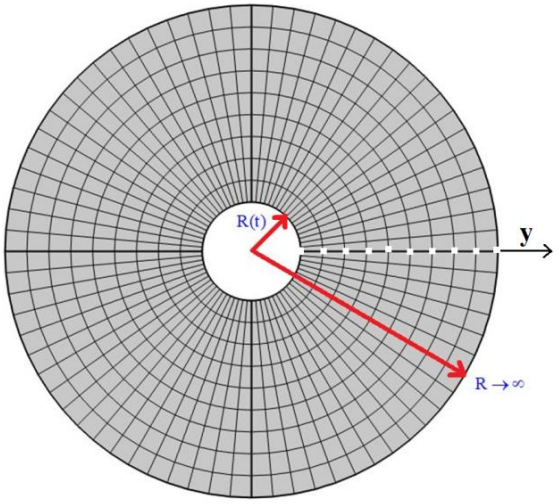

Fig. A1 Schematic showing the spherical bubble and the spherical computational domain discretized using a coarse mesh. Much finer mesh is used in practice for the true simulations. The nodes needed for the simulations are drawn

12) to this solver by writing appropriate scripts. It is also required to discretize the domain. Figure A1 shows a typical domain, which is normally used for two- or three-dimensional flows. Fortunately, the problem at hand is one-dimensional meaning that one needs to do is to put sufficient nodes along an arbitrary radius (e.g., *y*-direction shown in Fig. A1) and then activate the solver. Deciding on the number of nodes needed for the results to be grid-independent is something very important that is discussed below. For spatial discretization of the transport equation for the structural parameter, we have used Lagrange shape functions based on quadratic type of elements in this software. To temporally discretize the system of equations, we have used fully-coupled version of the time-dependent solver based on the Non-Linear Newton iterative method (using a damping factor of 1). The method uses implicit discretization in an iterative manner where the stability of the simulation needs to be significantly improved for situations where bubble deformation is large (e.g., during its chaotic response).

It is worth-mentioning that in the present study selecting an optimum value for the far-field radius (R_{max}), i.e., the radius representing physical infinity turned out to be a tedious but straightforward task. The idea was to check the structural parameter at the chosen R_{max} to see if it meets the criterion that the fully-rebuilt condition (S = 1) is met for the Quemada model. To achieve this goal we have tested different values for R_{max} in our simulations and reached to the conclusion that to meet this boundary condition, it is sufficient to set far field radius at least 100 times the bubble's initial radius. To ensure mesh-independency, however, it was found that $R_{max} = 400R_0$ is a conservative option. So, in the simulation results reported in the main body of the paper, use was made of this value. From another perspective, to increase accuracy of the simulated results, particularly in cases where the bubble behaves chaotically, we have increased the resolution of the mesh grids near the bubble's surface. To do this, we have used 2000 elements with element ratio of 1.75 in the whole computational domain.

Appendix B: Gauss-Laguerre Method

The Gauss–Laguerre quadrature method has been used in the past for simulating bubble dynamics in thixotropic fluids (Kafiabad & Sadeghy, 2010). The method is based on the premise that the stress field decays exponentially in the radial direction. As the first step, by substituting $y = r - R(t)$ the bubble's wall is immobilized, so that Eq. 9 is transformed from the Eulerian framework to the Lagrangian framework. The fluid's domain is then divided such that the first point always corresponds to the bubble wall—this little maneuvering eliminates the need for following a moving boundary. Based on this scheme, the structural parameter is always set equal to 1 at the last grid point. In other words, at far-field, the fluid's microstructures remains intact so that $S(t,\infty) = 1$ at all times. The initial conditions are:

$$R(0)=1\,,\ \dot{R}(0)=0\ ,\ S(0,r)=1. \tag{B1}$$

For solving the governing equations, use was made of the MATLAB software. To that end, the domain is discretized into N points in such a way that the first point corresponds to the bubble wall. The discretized system is as follows:

$$\frac{dR}{dt}=U\,, \tag{B2}$$

$$\frac{dU}{dt}=\frac{1}{R}\left[-\frac{3}{2}U^2+C_P\left[(1+We)\right]\left(\frac{1}{R}\right)^{3\kappa}-C_P\left(1+\varepsilon\,sin(t)\right)-C_P\frac{We}{R}\right]- 12\,\frac{R^2U}{Re}\int_0^{\infty}\frac{(1+\alpha\ S(y,t))^{\beta}}{(y+R)^4}dy\,. \tag{B3}$$

The last equation to be discretized is the structural parameter transport equation, i.e., Eq. 12. To that end, Eq. (12) is transformed from the r-t plane to the y-t plane using the transformation: $y = r - R(t)$. After some mathematical manipulations, the following transformed equation is obtained:

$$\lambda\frac{\partial S}{\partial t}+\lambda\dot{R}\left[\frac{R^2}{(y+R)^2}-1\right]\frac{\partial S}{\partial y}= -Rx\ (12)^{n/2}\frac{\dot{R}^nR^{2n}}{(y+R)^{3n}}S +(1-S)\ (12)^{m/2}\frac{\dot{R}^mR^{2m}}{(y+R)^{3m}}. \tag{B4}$$

The above equation is valid in the range of $0 \le y \le \infty$. To couple this equation with Eqs. B2 and B3, it is required that Eq. B4 is discretized in each spatial position y. If $1 \le j \le N$ represents $0 \le y \le \infty$ then discretization of Eq. B4 can be written as:

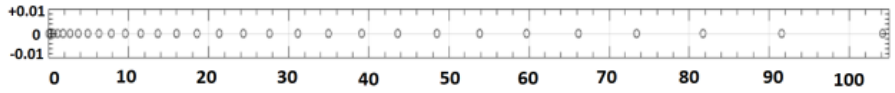

Fig. B1 A typical grid used in the Gauss-Laguerre quadrature method. The nodes are seen to be concentrated near the surface of the bubble (y = 0)

$$\left.\frac{dS}{dt}\right|_j = -U\left[\frac{R^2}{\left(y_j+R\right)^2}-1\right]\left.\frac{\partial S}{\partial y}\right|_j - \frac{Rx}{\lambda}(12)^{\frac{n}{2}}\frac{U^n R^{2n}}{\left(y_j+R\right)^{3n}}S + \left(\frac{1-S}{\lambda}\right)(12)^{m/2}\frac{U^m R^{2m}}{\left(y_j+R\right)^{3m}}. \quad \text{(B5)}$$

where we have:

$$\left.\frac{\partial S}{\partial y}\right|_j = \begin{cases} \dfrac{S_{j+1}-S_j}{y_{j+1}-y_j} & ;\quad \mathrm{j}=1 \\ K_{j-1}S_{j-1}+K_jS_j+K_{j+1}S_{j+1} & ;\ 2\le \mathrm{j}\le \mathrm{N}-1 \\ \dfrac{\cancel{S_j}^{1}-S_{j-1}}{y_j-y_{j-1}} & ;\quad \mathrm{j}=\mathrm{N} \end{cases} \quad \text{(B6)}$$

where K_{j-1}, K_j and K_{j+1} are defined as:

$$\begin{cases} K_{j-1} = -\dfrac{y_{j+1}-y_j}{(y_j-y_{j-1})^2\left(1+\dfrac{y_{j+1}-y_j}{y_j-y_{j-1}}\right)} \\ K_j = \dfrac{\dfrac{y_{j+1}-y_j}{y_j-y_{j-1}}-1}{y_{j+1}-y_j} \qquad ;\ 2\le \mathrm{j}\le N-1 \\ K_{j+1} = \dfrac{1}{(y_{j+1}-y_j)\left(1+\dfrac{y_{j+1}-y_j}{y_j-y_{j-1}}\right)} \end{cases} \quad \text{(B7)}$$

Moreover, S_N has been replaced by 1 due to boundary condition at far field on S. The initial conditions are: R(0) = 1, $U(0)$ = 0 and $S_j(0)$ = 1. These equations are then solved numerically using the Gauss-Laguerre method. To that end, the integral in Eq. B3 is approximated as:

$$I \approx \sum_{k=1}^{N} w_k \varphi(y_k), \quad \text{(B8)}$$

where y_k are the zeros of the Laguerre polynomials, which are defined as (Jaluria, 1988):

$$L_n(x) = e^x \frac{d^n}{dx^n}\left(e^{-x}x^n\right) \quad \text{(B9)}$$

Also, are the weighting functions related to the Laguerre polynomials as:

$$w_i = \frac{(n!)^2}{x_i\left(L_n'(x_i)\right)^2} \quad \text{(B10)}$$

What remains to be done is to discretize the domain using the roots of the Laguerre polynomials, which has been shown in Fig. B1 where the domain has been discretized using N = 30 nodes with y = 104.175 serving as the node representing physical infinity. The nodes are seen to be concentrated near the bubble surface so that sharp variation in the stress terms can be resolved; see Kafiabad and Sadeghy (2010) for more details.